Lab on a Chip

RSC Publishing

PAPER

View Article Online
View Journal | View Issue

Hybrid optofluidic integration†

Cite this: *Lab Chip*, 2013, **13**, 4118

Joshua W. Parks,‡[a] Hong Cai,‡[a] Lynnell Zempoaltecatl,[b] Thomas D. Yuzvinsky,[a] Kaelyn Leake,[a] Aaron R. Hawkins[b] and Holger Schmidt*[a]

Received 9th July 2013,
Accepted 25th July 2013

DOI: 10.1039/c3lc50818h

www.rsc.org/loc

Complete integration of microfluidic and optical functions in a single lab-on-chip device is one goal of optofluidics. Here, we demonstrate the hybrid integration of a PDMS-based fluid handling layer with a silicon-based optical detection layer in a single optofluidic system. The optical layer consists of a liquid-core antiresonant reflecting optical waveguide (ARROW) chip that is capable of single particle detection and interfacing with optical fiber. Integrated devices are reconfigurable and able to sustain high pressures despite the small dimensions of the liquid-core waveguide channels. We show the combination of salient sample preparation capabilities—particle mixing, distribution, and filtering—with single particle fluorescence detection. Specifically, we demonstrate fluorescent labelling of λ-DNA, followed by flow-based single-molecule detection on a single device. This points the way towards amplification-free detection of nucleic acids with low-complexity biological sample preparation on a chip.

Introduction

The original motivation for a lab-on-a-chip was to unite as many functions in a single chip-scale device as possible.[1] Typically, this includes both chemical or biological sample preparation and optical or electronic sample analysis. This presents considerable challenges since the materials that have been optimized for these tasks—polymers and glass for sample preparation; semiconductors for optoelectronic detection—are very different. In addition, the growing need for genomic and proteomic molecular analyses at low concentrations and volumes such as in single-cell analysis requires extremely high sensitivities.[2]

The growing area of optofluidics[3–5] offers a path towards accomplishing these goals by combining microfluidics and integrated optics in a single lab-on-a-chip system. It was pointed out early on[3,6] that one particularly attractive optofluidic approach could involve the vertical integration of dedicated fluidic and optical layers, each optimized independently and suitably interfaced with the other.

Here, we introduce the concept of hybrid optofluidic integration that combines the strengths of microfluidic sample handling in PDMS microchannels with single particle optical detection sensitivity in silicon-based liquid-core waveguide chips. Its core features are reconfigurability *via* a non-permanent interface, small dead volume, optical planarity that allows for vertical integration as shown in Fig. 1, and single-particle optical sensitivity afforded by the use of liquid-core antiresonant reflecting optical waveguides (ARROWs).[7–11]

The key steps for preparing a complex biological sample based on whole blood, saliva, *etc.* for on-chip optical analysis include the removal of large matrix components that could clog the waveguide channels, labeling with target-specific optical markers, and distribution into multiple optical channels for multiplex detection. We demonstrate the compatibility of all three canonical functions (mixing, filtering, distribution) with analysis on an ARROW chip and characterize the fluid transport properties of the integrated device. Specifically, we implement for the first time the combination of on-chip labeling of λ-DNA, followed by single molecule DNA detection in the optical layer. This assay indicates that amplification-free detection of nucleic acids starting with raw sample material is feasible.

Materials and methods

The underlying optical technology for the hybrid, integrated system is based on liquid-core antiresonant reflecting optical

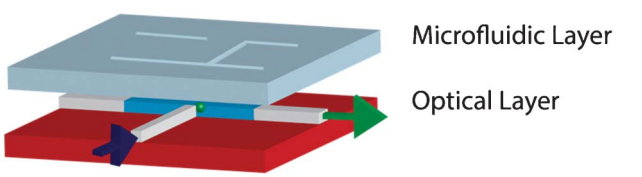

Fig. 1 Schematic depiction of hybrid optofluidic integration of microfluidic sample preparation (top) and optical analysis (bottom) layers.

[a]*School of Engineering, University of CA Santa Cruz, 1156 High Street, Santa Cruz, CA, 95064, USA. E-mail: hschmidt@soe.ucsc.edu; Fax: +1-831-459-4829; Tel: +1-831-459-1482*

[b]*ECEn Department, Brigham Young University, Provo, UT, 84602, USA*

† Electronic supplementary information (ESI) available. See DOI: 10.1039/c3lc50818h

‡ These authors contributed equally to this work.

waveguides (LC-ARROWs).[7,8] These consist of micron-scale hollow channels that are clad with thin dielectric layers of appropriate thickness to provide optical confinement in the low-index core at desired wavelengths.[9] LC-ARROWs can be interfaced with solid-core waveguide sections that allow light to be guided to and from the liquid-core sections with high coupling efficiency.[12,13] This principle has been used to demonstrate particle pushing,[14] trapping,[15] Raman scattering[16] and fluorescence detection with single particle sensitivity[10,11,14,17] on a chip. The most important characteristic of this platform in the context of optofluidic integration is its optical planarity, *i.e.* all optical signals propagate exclusively in the plane of the chip, leaving the third dimension for addition of a microfluidic sample processing layer.

ARROW chips were fabricated using optimized procedures previously described.[12,13,18,19] The wavelength response of these chips was designed using a 2 × 2 matrix formalism[9,20] to create low-loss propagation between 400 and 800 nm. Optimized SiO_2 (refractive index $n = 1.47$) and Ta_2O_5 ($n = 2.107$) ARROW layers were deposited by Evaporated Coatings Inc. on a silicon wafer. The layers were deposited in an alternating fashion, starting with SiO_2, at thicknesses of 265/102/265/102/265/102 nm. The liquid-core waveguide was defined lithographically to nominal cross-section dimensions of 12 × 5 μm (width × height). An SiO_2 thin film overcoat of 6 μm thickness was used to create the channel.[12] Solid-core ridge waveguides for delivery and collection of optical signals were formed in the top oxide overcoat *via* reactive ion etching with a width of 4 μm and etch depth of 3 μm. The layout of the final "ARROW Chip" is shown in Fig. 2a (footprint 8 × 8 mm). Scanning electron microscope images are presented for both the excitation and collection intersection between the liquid and solid core waveguides.

PDMS channels for the microfluidic layer were formed using conventional soft lithography.[21,22] Master molds for channels of 30 μm height and widths from 75 to 200 μm were lithographically defined using SU-8 negative photoresist. PDMS elastomer and curing agent were mixed in a 10 : 1 ratio and degassed for one hour, after which the mixture was poured onto the silanized SU-8 master and baked for one hour at 60 °C.

Manifold, or access, layers—as shown in Fig. 2a—were bonded according to material type. For access layers made of glass or PDMS, the manifold and microfluidic PDMS layers were bonded using a 30 W oxygen plasma treatment for 30 s. For polycarbonate access layers, a preliminary APTES treatment was used to activate the surface before oxygen plasma bonding.[23]

To perform the hybrid integration between a PDMS microfluidic device and an ARROW optofluidic chip, we implemented an approach using metal reservoirs (2 mm outer diameter, Fire Mountain Gems) that were inserted into holes punched into the PDMS layer. The natural concavity of the punch holes results in an excellent airtight seal with the reservoirs. Subsequently, epoxy was applied to the lower reservoir edges, and finally the entire device was assembled

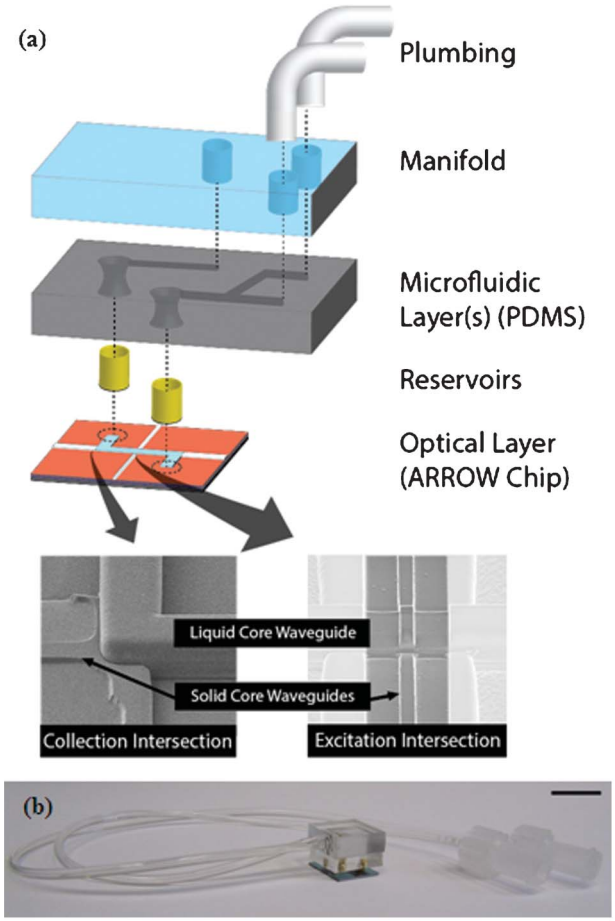

Fig. 2 (a) Expanded view of PDMS integration with an ARROW optofluidic chip. Insets are scanning electron microscope (SEM) images of optical intersections. (b) Assembled device with fluidic connections (scale bar in the upper right represents 1 cm).

by lowering the fluidic chip onto the optical chip using a micromanipulation stage. At this point, the epoxy was allowed to cure overnight to ensure device stability. It is important to note that the PDMS layer is not in contact with the ARROW chip and thus optical guiding properties are inherently conserved. Furthermore, while the PDMS-reservoir interface is stable under very high pressures, it is also reconfigurable due to the lack of permanent adhesive. In other words, after the device has been completed, the PDMS microfluidic assembly can be removed/replaced by simply pulling it off, leaving the aligned reservoirs in place. An alternative, more permanent approach using a punched 200 μm thin PDMS gasket layer to replace the reservoirs was also tested. In that case, the gasket layer was plasma-bonded to both the top of the ARROW chip and the bottom of the microfluidic PDMS layer. The results presented in the remainder of this work were obtained using the non-permanent reservoir interface.

Control of the liquid flow through the integrated device was realized externally using custom Luer lock syringe based actuators. Tygon tubing was used to connect the PDMS microfluidic chip to a 1 mL Luer lock syringe. Both ends of

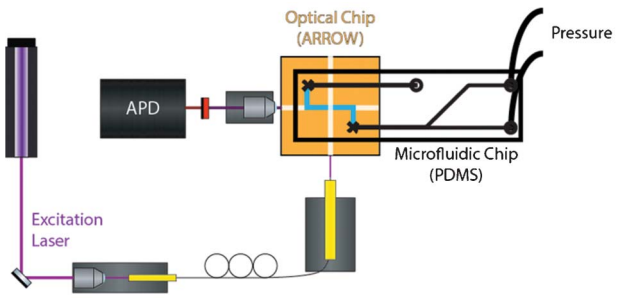

Fig. 3 Schematic of optical setup for microfluidic controlled particle detection.

the tubing were press-fit, providing a strong seal while retaining re-configurability. Finally, the syringe was immobilized in a custom mount and a micrometer screw was used to actuate flow in mixing and distribution experiments. For experiments that required a more controlled velocity, a syringe pump was used to actuate flow (Pump 11 Elite, Harvard Apparatus).

The detection setup implemented for optical particle analysis with fluidic control is seen in Fig. 3. An excitation laser (632.8 nm HeNe laser or 488 nm Ar-ion laser) was coupled into single mode fiber, which was in turn butt coupled into the ARROW chip with optical access from 3 sides as seen in Fig. 3. The waveguide output power was monitored straight across the chip to ensure stable coupling. The fluorescence signal was collected orthogonally and spectrally separated onto an avalanche photodiode and analyzed as previously described.[10,11,24]

Experimental solutions contained 0.1 mg mL^{-1} BSA (New England BioLabs) and 0.05% Tween20 (Fisher) as dynamic surfactants to inhibit aggregation and wall binding. Sodium azide was added at a final concentration of 5 μM to all solutions to retain biological purity.

Results and discussion

Flow properties

As the cross-sectional dimensions of the microfluidic and liquid-core waveguide channels are dramatically different, we first considered the flow properties of the integrated device. The fluidic resistance of a micro-channel is well approximated (less than 1% error for aspect ratios over 2) by the following equation[25]

$$R = \frac{12\eta L}{wh^3\left(1-0.630^{h}/_{w}\right)} \quad (1)$$

where η is the viscosity of the fluid, L is the length, w is the width of the channel, and h is the height. By substituting the dimensions of PDMS (75 × 30 μm, L = 8 mm) and ARROW liquid-core waveguide (12 × 5 μm, L = 4 mm) channels, fluidic resistances of R_{ARROW} = 43.48 cP μm^{-3} and R_{PDMS} = 0.0635 cP μm^{-3} are calculated. It is clear the resistance of the ARROW chip is about 700 times that of the PDMS channels. As the resistance scales linearly with channel length, a PDMS channel would need to be ~5 m long to match the impedance of typical ARROW chips. This implies that for typical chip dimensions, the fluidic resistance will always be dominated by the ARROW optical device layer, particularly since this simplified model does not account for the 90° bends in the ARROW liquid-core waveguide that further increase the resistance. Here we note the robustness of the reservoir bonding method to withstand large impedance mismatches and pressure differentials while remaining reconfigurable. For example, the maximum flow speed achieved was approximately 3 cm s^{-1} (as measured by top down video tracking of particles) corresponding to a flow rate of 0.108 μL min^{-1}. Accordingly, the pressure drop across the device (calculated from flow rate multiplied by fluidic resistance) was 78.3 kPa, and no leakage was observed.

On-chip mixing, labelling and detection of single DNA

A key step in a fluorescence assay is labeling the target with an optical marker. To this end, the raw sample must be brought in contact with the label. Here, we demonstrate mixing of λ-DNA with intercalating SYBR Gold fluorescent dye in the microfluidic layer, followed by detection of single, labeled λ-DNA molecules in the optical layer. Molecules were then excited with 488 nm laser light and detected as depicted above. It can be seen in Fig. 3 that the λ-DNA (New England Biolabs) and SYBR Gold (Invitrogen) are input into separate inlets on the microfluidic layer. In this layer, the two channels meet, the solutions mix, and are sent to the inlet of the optical layer for analysis.

A resultant time dependent fluorescence trace obtained by excitation with a 488 nm laser is presented in Fig. 4a. The dashed horizontal line shows the threshold level above the background, defined here as 3σ (three times the standard deviation) of a SYBR Gold control signal. Fluorescence peaks representing single λ-DNA molecules are present throughout the time trace—well above the noise threshold. A zoomed-in section (inset of Fig. 4a) unambiguously displays the individual fluorescence signals. Differences in signal strengths between individual nucleic acids are caused by an inhomogeneous labeling efficiency and the spatially dependent velocity[25] (Poiseuille flow) and collection efficiency[11] of the liquid-core waveguide. However, as this is a direct detection experiment (of single nucleic acids above a background threshold), the variation in signal strengths does not affect the assay.

λ-DNA time traces were subjected to fluorescence correlation spectroscopy (FCS) analysis. The experimental autocorrelation plot shown in Fig. 4b is presented along with a fitted curve based on a previously described model that accounts for both diffusion and flow,[26] and matches the data very well. For this FCS trace, G(0) is fit to approximately 2.4, corresponding to a concentration of 8.8 pM which is in reasonable agreement with the nominal diluted concentration of 12.5 pM, confirming the detection of single nucleic acids. Furthermore, the fitted value for flow speed is 6.8 mm s^{-1} further verifying the

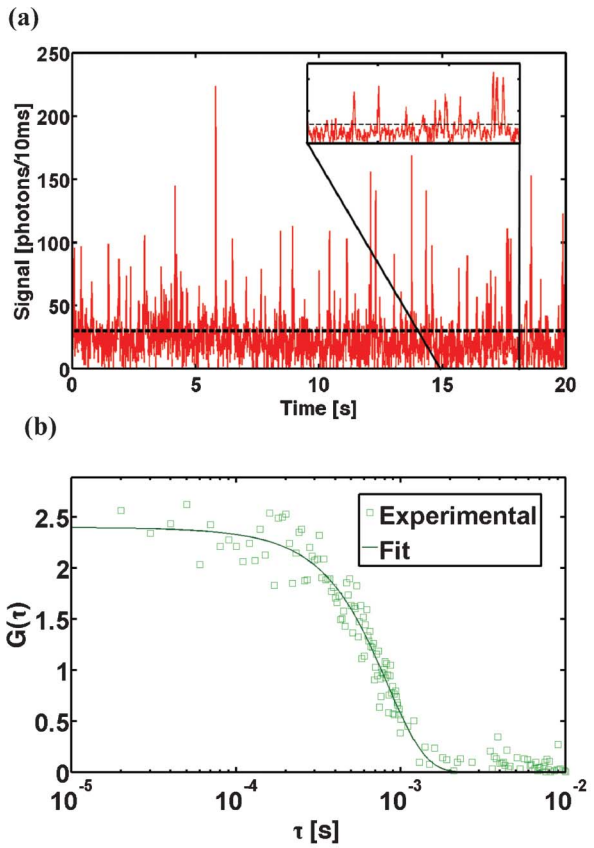

Fig. 4 (a) Time dependent fluorescence trace of on-chip mixed, labelled, and detected single λ-DNA molecules. The dashed black lines represent 3σ (three times the standard deviation of the noise) and the inset displays single detection events. (b) Experimental FCS trace of detected λ-DNA molecules (squares) and respective theoretical fit (line).

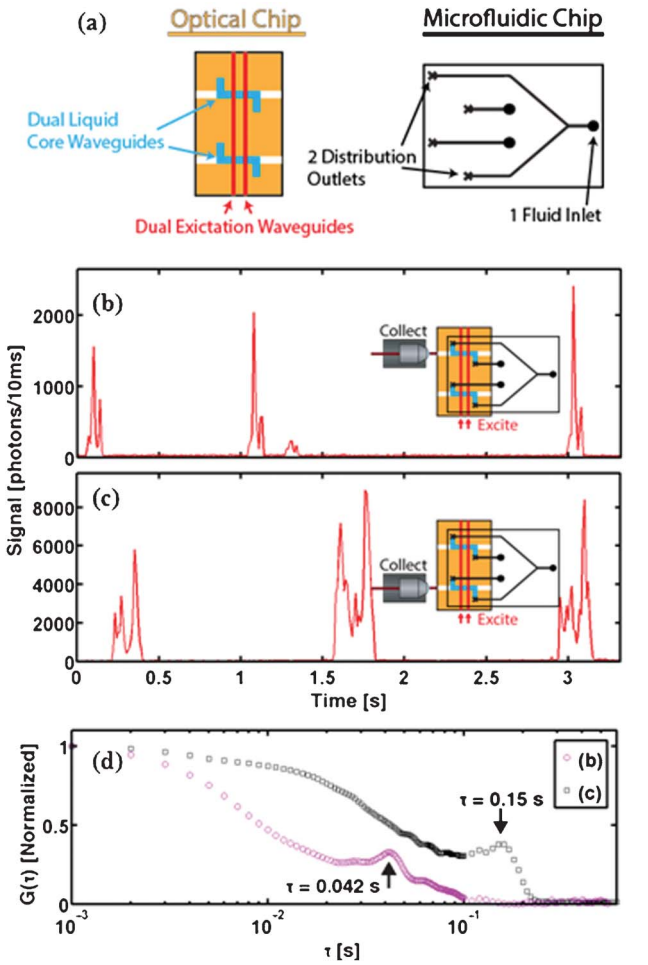

Fig. 5 (a) PDMS distribution with dual liquid-core waveguide detection. Signals were detected from liquid-core waveguide 1 (b) and 2 (c) separately while the same PDMS distribution device fluidically controlled both channels. (d) FCS analysis of both time trace signals. Local maxima are marked.

ability of the device to withstand high fluid velocities and respective pressures.

Microfluidic sample distribution

On-chip sample distribution is another important component of a lab-on-chip device as it enables multiplex detection in several ARROW channels and increases fluidic throughput. In this work, we implement a 1-in-2 splitter in the PDMS layer in order to distribute sample analyte from a single inlet into two optofluidic channels as seen in Fig. 5a. The particular dual liquid-core ARROW chip used in this experiment has two solid-core waveguides that are excited simultaneously (see Fig. 5a and red arrows in Fig. 5b and c insets) to yield a double Gaussian excitation profile for direct determination of the flow velocity (see below). These excitation waveguides extend across the entire chip and thereby provide simultaneous optical excitation of both liquid-core waveguides. For the collection of fluorescence signals, an objective was aligned sequentially to the top and bottom collection waveguides as illustrated in Fig. 5. After injecting crimson microspheres *via* a single PDMS input, 632.8 nm He-Ne light was used to excite the analytes.

Both data traces in Fig. 5 have characteristic doublets indicative of a double Gaussian excitation. The maximum signal for each doublet is lower in Fig. 5b than that in Fig. 5c because the excitation light experiences some attenuation between the first and second liquid channels. We note this is a result of lossy propagation and intersection scattering, both of which have no effect on single particle detection.[11] Such losses result in respectively smaller fluorescence signals in the channel more distant from the excitation source. For this same reason, the imperfections in the double Gaussian signals of Fig. 5c—caused by leakage of excitation light in the cladding of solid-core waveguides—are not apparent in Fig. 5b. Further analysis shows that the first peak of each doublet in Fig. 5b, and the second of each doublet in Fig. 5c, are larger in amplitude than their respective partners due to uneven power distribution between the excitation waveguides, and the fact that injection into the ARROW channel occurs from opposite ends (see Fig. 5). Finally, as the spacing between the maxima of the two excitation waveguides is well defined, an easy, direct, and accurate velocimetry analysis can be performed. By taking the spacing of the excitation waveguides (25 μm) and dividing it by the temporal spacing of each doublet, the

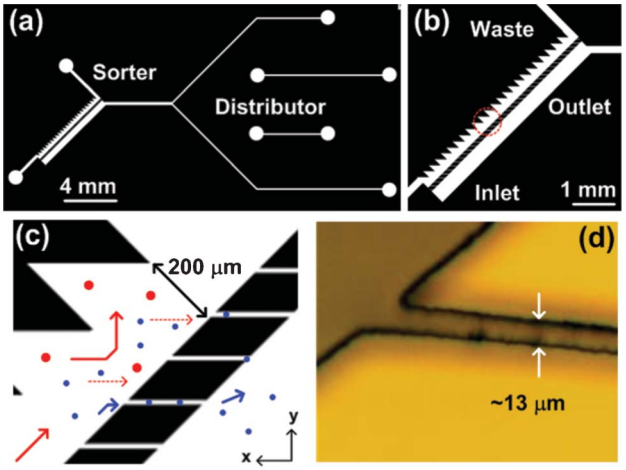

Fig. 6 (a) Mask layout of the PDMS sorter and distributor. (b) Zoomed-in view of the particle size sorter section. (c) Zoomed-in view of the filtering membrane and the corrugated walls inside the inlet channel. (d) Microscope image of the fabricated PDMS filtering membrane slit.

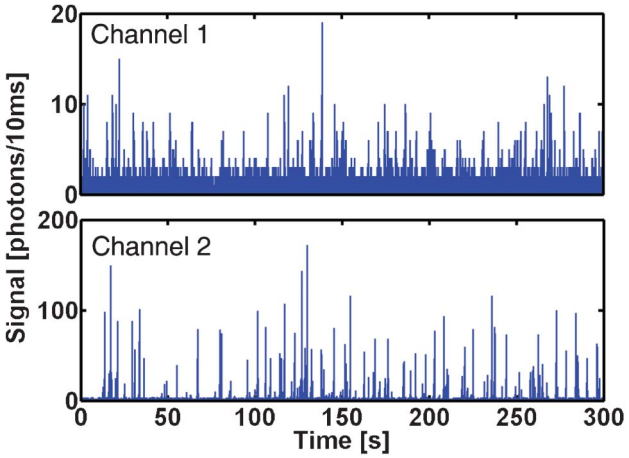

Fig. 7 PDMS filtering and distribution with dual liquid-core waveguide detection. Signals were detected from liquid-core waveguides 1 and 2 with an input flow rate at ~2 μl min^{-1}.

magnitude of the velocity was determined to be 600 μm s^{-1} for particles in Fig. 5b and 170 μm s^{-1} for particles in Fig. 5c. Similarly, upon performing FCS analysis on these traces, there is a local maximum at lags equal to the time between peaks—as seen in Fig. 5d—that is in excellent agreement with the direct measurement, and thus confirming this technology as an accurate flow sensor. The difference in flow velocities is attributed to a hole in the epoxy sealing one of the ARROW chip-reservoir interface. This highlights the possibility of differential control of the channel velocities *via* a pressure release system or channel dimensions that produce different fluidic resistance. Even without differential control, this is the first presentation of multiplexed liquid-core waveguide detection with a single optical source.

Microparticle filtering and distribution

A third important fluidic sample processing capability is size-based particle filtering and selection. In our hybrid optofluidic system, such a step is critical to prevent particles of more than a few microns diameter, *e.g.* cells or cell fragments, from clogging the small channels of the ARROW chip.

Fig. 6a shows the mask layout of the sorter which we combined with a 1-in-2 distributor section as described above. Fig. 6b and Fig. 6c show a zoomed-in view of the sorter which consists of a corrugated wall in the input channel and a micro-slit filtering membrane separating the inlet/waste and outlet channels.[27] A particle mixture (diameters 1 and 15 μm) is injected from the inlet channel. The mixed solution generally travels from the inlet of the sorter to outlet. The corrugated wall in the input channel helps to deflect the particles towards the filtering membrane by creating a two-dimensional flow (the flow direction is indicated by red and blue arrows in Fig. 6c) and thus creates another pressure gradient in the *x-y* plane (indicated by red-dashed arrows in Fig. 7c). Particles smaller than the slit opening pass through the membrane and enter the outlet channel for secondary processing (which in this case means distribution into the two ARROW channels for fluorescence detection). Particles with sizes greater than the slit opening will continue to flow forward to the waste output, as illustrated in Fig. 6c. The gap between the corrugated wall and the filtering membrane was chosen to be 200 μm. Fig. 6d shows a microscope image of the fabricated PDMS filtering membrane. The fabricated filtering slit width is 13 μm in order to block 15 μm particles. For a commercialized plastic photolithography mask, we are able to transfer a filtering slit down to ~6 μm wide which is limited by the commercial printer. With laser-defined chrome masks, submicron resolution is achievable. Such resolution is sufficient to block larger sized components of biological samples from clogging the ARROW channel, an example of which is filtering red blood cells from whole blood.

In this experiment, a detection scenario similar to that seen in Fig. 5 was implemented. Two notable differences include a single excitation waveguide and the use of a syringe pump. After injecting a mixture of 1 μm (Invitrogen) and 15 μm (Polysciences) diameter microspheres *via* the PDMS layer into the ARROW chip, a 488 nm Ar-ion laser was used to excite the filtered particles. Video 1 (see ESI†) shows the movement of 1 μm and 15 μm particles inside the microfluidic channel with an input flow rate of 1 μl min^{-1} as an example.

Fig. 7 shows the detected fluorescence signal from ARROW channels 1 and 2 with the input flow rate of the sorter set to 2 μl min^{-1}. The particle injection rates inside the ARROW channels were recorded as 0.33 particles per second and 0.37 particles per second for channel 1 and 2, respectively. Note the ARROW chip inlets are completely sealed and the flow velocities in each channel are very similar.

The large microbeads were prevented from reaching the ARROW channel with 100% efficiency. In order to determine the sorting efficiency for 1 μm particles, aliquots of experimental solution were subjected to flow cell cytometry. The prepared 1 μm particle concentration was measured to be 3.25 × 10^7 particles per ml. The 1 μm particle concentration collected at the waste output during the experiment was found

to be 2.37 × 10^7 particles per ml. Therefore, the sorting efficiency for the 1 μm particles is 33.5%. This value can be increased by repeated cycling through the sorter section and by optimizing the dimensions of the sorter section, such as the period of the corrugated wall, the angle of the slits, and the gap distance.

Conclusions

We have introduced a method for the hybrid integration of dedicated fluidic sample processing and high sensitivity optical analysis in a single optofluidic system. Vertical integration using non-permanent, reconfigurable interfacing *via* reservoirs provides a means of retaining optical viability of liquid-core ARROW waveguides while allowing for closed integration with microfluidic PDMS layers. The interfacing provides excellent sealing even at high pressures despite large fluidic impedance mismatches between the optical and microfluidic layers. Three capabilities that will form part of a complete chip-scale bioanalysis device—fluidic mixing, distribution, and filtering—were presented. In particular, the combination of fluorescent dye labelling with fluorescence detection of single λ-DNA molecules was demonstrated.

The independence of the fluidic layer design will allow for future hybrid integration with more complex microfluidic technologies based on actively controlled valves.[28–30] These examples of integrated sample processing and detection are important steps towards complete lab-on-a-chip analysis. They point towards the possibility of comprehensive molecular analyses such as amplification-free nucleic acid testing using small input volumes of biologically and chemically complex sample materials.

Acknowledgements

The authors thank Shuo Liu for his contribution to flow control and Brandon Carter at the MEGAMER facility for his assistance with flow cell cytometry. We also recognize P. Lum, P. Marshall, J. Peterson, and P. Measor for fruitful discussions and initial contributions. This work was supported by the National Science Foundation under grant number CBET-1159453 and CBET-1159423, the National Institutes of Health under grant NIH R21 AI100229, the California Institute for Quantitative Biosciences (QB3), and the W.M. Keck Center for Nanoscale Optofluidics at the University of California at Santa Cruz. J.W.P. acknowledges support by the National Science Foundation Graduate Research Fellowship Program under grant DGE 0809125.

References

1 A. Manz, N. Graber and H. M. Widmer, *Sens. Actuators, B*, 1990, **1**, 244–248.
2 B. Huang, H. Wu, D. Bhaya, A. Grossman, S. Granier, B. K. Kobilka and R. N. Zare, *Science*, 2007, **315**, 81–4.
3 D. Psaltis, S. R. Quake and C. Yang, *Nature*, 2006, **442**, 381–6.
4 X. Fan and I. M. White, *Nat. Photonics*, 2011, **5**, 591–597.
5 H. Schmidt and A. R. Hawkins, *Nat. Photonics*, 2011, **5**, 598–604.
6 D. Erickson, T. Rockwood, T. Emery, A. Scherer and D. Psaltis, *Opt. Lett.*, 2006, **31**, 59–61.
7 M. Duguay, Y. Kokubun, T. Koch and L. Pfeiffer, *Appl. Phys. Lett.*, 1986, **49**, 13–15.
8 D. Yin, D. W. Deamer, H. Schmidt, J. P. Barber and A. R. Hawkins, *Appl. Phys. Lett.*, 2004, **85**, 3477.
9 D. Yin, J. Barber, A. R. Hawkins and H. Schmidt, *Opt. Express*, 2005, **13**, 9331–6.
10 D. Yin, D. W. Deamer, H. Schmidt, J. P. Barber and A. R. Hawkins, *Opt. Lett.*, 2006, **31**, 2136–8.
11 D. Yin, E. J. Lunt, M. I. Rudenko, D. W. Deamer, A. R. Hawkins and H. Schmidt, *Lab Chip*, 2007, **7**, 1171–5.
12 E. J. Lunt, P. Measor, B. S. Phillips, S. Kühn, H. Schmidt and A. R. Hawkins, *Opt. Express*, 2008, **16**, 20981–6.
13 Y. Zhao, K. Leake, P. Measor, M. Jenkins and J. Keeley, *IEEE Photonics Technology Letters*, 2012, **24**, 46–48.
14 P. Measor, S. Kühn, E. J. Lunt, B. S. Phillips, A. R. Hawkins and H. Schmidt, *Opt. Lett.*, 2008, **33**, 672.
15 S. Kühn, P. Measor, E. J. Lunt, B. S. Phillips, D. W. Deamer, A. R. Hawkins and H. Schmidt, *Lab Chip*, 2009, **9**, 2212–6.
16 P. Measor, L. Seballos, D. Yin, J. Z. Zhang, E. J. Lunt, A. R. Hawkins and H. Schmidt, *Appl. Phys. Lett.*, 2007, **90**, 211107.
17 S. Kühn, B. S. Phillips, E. J. Lunt, A. R. Hawkins and H. Schmidt, *Lab Chip*, 2010, **10**, 189–94.
18 E. J. Lunt, B. Wu, J. M. Keeley, P. Measor, H. Schmidt and A. R. Hawkins, *IEEE Photonics Technol. Lett.*, 2010, **22**, 1147–1149.
19 Y. Zhao, M. Jenkins, P. Measor, K. Leake, S. Liu, H. Schmidt and a. R. Hawkins, *Appl. Phys. Lett.*, 2011, **98**, 91104.
20 P. Yeh, *Optical Waves in Layered Media*, John Wiley & Sons Inc., Hoboken, NJ, 1998.
21 D. C. Duffy, J. C. McDonald, O. J. Schueller and G. M. Whitesides, *Anal. Chem.*, 1998, **70**, 4974–84.
22 Y. Xia and G. Whitesides, *Annual Review of Materials Science*, 1998, **37**, 550–575.
23 K. S. Lee and R. J. Ram, *Lab Chip*, 2009, **9**, 1618–24.
24 A. Chen, M. M. Eberle, E. J. Lunt, S. Liu, K. Leake, M. I. Rudenko, A. R. Hawkins and H. Schmidt, *Lab Chip*, 2011, **11**, 1502–6.
25 H. Bruus, *Theoretical Microfluidics*, Oxford University Press, New York, NY, 2007.
26 M. I. Rudenko, S. Kühn, E. J. Lunt, D. W. Deamer, a. R. Hawkins and H. Schmidt, *Biosens. Bioelectron.*, 2009, **24**, 3258–63.
27 J. G. Fernandez, C. a. Mills, R. Rodríguez, G. Gomila and J. Samitier, *Phys. Status Solidi A*, 2006, **203**, 1476–1480.
28 E. C. Jensen, B. P. Bhat and R. A. Mathies, *Lab Chip*, 2010, **10**, 685–91.
29 J. Kim, M. Kang, E. C. Jensen and R. A. Mathies, *Anal. Chem.*, 2012, **84**, 2067–71.
30 M. Unger, H. Chou, T. Thorsen, A. Scherer and S. Quake, *Science*, 2000, **288**, 113–6.